Chapter 4

4 THE DETERMINATION OF OPTIMUM PLATFORM GEOMETRIES FOR PRESCRIBED MACHINING TASKS

4.1 Introduction

Du Plessis et al. [70] introduced the unique concept of an *adjustable geometry* planar Gough-Stewart platform machining center, where the geometry of the planar machining center is *optimized* using the LFOPC-algorithm [64]. The geometry was optimized with respect to the *static actuator forces* required to hold the mechanism in static equilibrium at each instant along the prescribed path. The *dynamic actuator forces* were also taken into account in the work by Snyman and Smit [71], in which the manipulator dynamics were simulated using the *Dynamic Analysis Design System* (DADS v. 9.0) [72]. They found that optimizing the platform geometry using the DADS software for the dynamics was computationally expensive if excessive numerical noise in the objective functions was to be avoided.

This chapter now explains how the LFOPC-algorithm [64] may be used to *optimize* the adjustable geometry of the planar Gough-Stewart platform machining center for any reasonably prescribed path using the stand-alone and *fundamentally based inverse dynamic analysis* procedure developed in **Chapter 2**. Here the actuator forces are determined as the manipulator moves in a prescribed manner along the specified path. In this study, the path specification is done using to the OCAS trajectory-planning methodology as explained in **Chapter 3**.

Minimizing the dynamic actuator forces required for executing the prescribed path with respect to the geometry, results in the avoidance of the very large actuator forces associated with singularities. Furthermore, as a by-product of the *constrained* optimization procedure, a *positioning* of the planar Gough-Stewart platform relative to the prescribed path is obtained that automatically ensures that the tool path is *feasibly placed* within the *workspace* of the mechanism. If it is not possible to place the prescribed path inside the workspace of the manipulator, the optimization algorithm yields an optimum compromised design geometry which allows the user to intervene in a rational manner.

Section 4.2 explains the formulation of the basic constrained optimization problem, while Section 4.3 gives details regarding the evaluation of the objective and constraint functions. The procedure for solving the optimization problem is explained in Section 4.4. Finally, the results of a representative optimization test run are shown and discussed in Section 4.5.

4.2 Formulation of the constrained optimization problem

In general, any conceptual design, dependent on n real *design variables* $\mathbf{X} = [X_1, X_2, X_3, \ldots, X_n]^T$, can be optimized by firstly defining an appropriate *objective function* $F(\mathbf{X})$, and where applicable, additional *inequality constraints* $C_j(\mathbf{X}) \leq 0$ $(j = 1,2,3,\ldots m)$ and *equality constraints* $H_k(\mathbf{X}) = 0$ $(k = 1,2,3,\ldots p < n)$. The optimum design $\mathbf{X}^*$ and optimum objective function value $F(\mathbf{X}^*)$ can then be found by applying any one of several available optimization techniques or algorithms, to solve the following mathematically formulated (constrained) optimization problem:

$$\begin{gathered}\underset{\mathbf{X}}{\text{minimize}}\ F(\mathbf{X}) \\ \text{with } \mathbf{X} = [X_1, X_2, X_3, \ldots, X_n]^T \\ \text{such that } C_j(\mathbf{X}) \leq 0 \quad j = 1,2,3,\ldots m \text{ and } H_k(\mathbf{X}) = 0\,;\ k = 1,2,3,\ldots p < n\end{gathered} \tag{4.1}$$

The selection of the design variables must be such that the objective function $F(\mathbf{X})$, the inequality constraint functions $C_j(\mathbf{X})$ $(j = 1,2,3,\ldots m)$ and the equality constraint functions $H_k(\mathbf{X})$ $(k = 1,2,3,\ldots p < n)$ are all dependent on $\mathbf{X} = [X_1, X_2, X_3, \ldots, X_n]^T$.

4.2.1 Design variables describing the adjustable geometry of the planar Gough-Stewart platform machining center

With reference to **Chapter 2**, where the planar Gough-Stewart platform machining center was introduced (see Figure 2.2 and 2.5), the positioning of the actuator joints on the base and on the moving platform may easily be adjusted. This feature is also incorporated in the practical design of the planar Gough-Stewart platform test-model with *continuously* adjustable geometry (see **Appendix D**). In particular the five design variables $\mathbf{X} = [X_1, X_2, X_3, X_4, X_5]^T$, indicated by the arrows in Figure 4.1, are used to describe the proposed adjustable geometry.

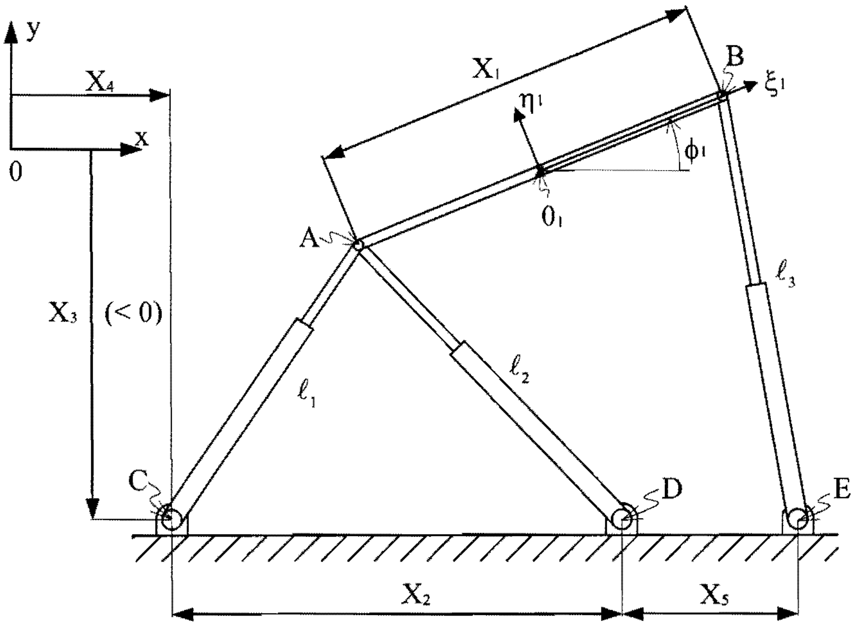

Figure 4.1: Five design variables describing the adjustable geometry planar Gough-Stewart platform machining center.

The two design variables X_3 and X_4 represent the coordinates of the left most revolute joint C on the horizontal base relative to the fixed global reference frame. In practical terms this implies that the position of point C on the base of the planar Gough-Stewart platform must be adjustable. This required positional adjustment may of course also be accomplished in practice by shifting the position of the global origin 0 relative to the fixed horizontal base (see Figure 2.8 and 2.10 for the *fixed workpiece* and *fixed cutting tool* cases respectively). The tool path is described relative to the global origin 0, and the kinematic and kinetic analysis of the mechanism is also done relative to its position (**Chapter 2**).

The remaining three design variables X_1, X_2 and X_5 indicate the relative distances between the linearly adjustable revolute joints of the fixed base (X_2 and X_5) and the moving platform (X_1).

In summary, and with reference to Figure 4.1,

$$\left|\xi_1^A\right| + \xi_1^B = X_1 \tag{4.2}$$

and

$$\begin{aligned} x^C &= X_4 & x^D &= X_4 + X_2 & x^E &= X_4 + X_2 + X_5 \\ y^C &= X_3 & y^D &= X_3 & y^E &= X_3 \end{aligned} \tag{4.3}$$

In order to solve for expression (4.2), one of the two local coordinates ξ_1^A or ξ_1^B must be known. If the center of mass of the moving platform is midway between revolute joints A and B, expression (4.2) reduces to $|\xi_1^A| = \xi_1^B = \dfrac{X_1}{2}$.

4.2.2 Objective function used to optimize the planar machining center geometry

The objective function used here, is the *overall maximum magnitude of the individual actuator forces* f_k, $k = 1,2,3$ (see expression (2.124)), as the planar Gough-Stewart platform moves along a prescribed tool path.

Using to the OCAS trajectory-planning algorithm, the prescribed path is specified by a set of nodal points $\{P_i = (x_i, y_i), i = 0,1,...,N\}$ (see Section 3.1). Time instants are then allocated to the consecutive nodal points according to the specified tangential "cutting speed", as well as the magnitude of the maximum allowable tangential acceleration. Each consecutive time span $[t_i, t_{i+1}]$, $i = 0,1,...,N-1$, with associated magnitudes $\Delta t_i = t_{i+1} - t_i$ is then subdivided into an additional number of equally spaced intermediate time instants, using the parameter n_{time} (see **Appendix B**). This intermediate time parameter is used in the OCAS-algorithm for the graphical representation of the results as is explained in Section 3.5.1.

In determining the overall maximum magnitude of the individual actuator forces f_k, $k = 1,2,3$, for a specific prescribed tool path, the additional *time discretization parameter* n_{time} is again utilized. This allows for a further discretization of the interval $[t_i, t_{i+1}]$ into time instants $t_{i,j} = t_i + \dfrac{j}{n_{time}} \Delta t_i$, $i = 0,1,2,...,N-1$, $j = 0,1,2,...,n_{time}$. Hence, for a sufficiently refined time discretization $\{t_{i,j}, i = 0,1,2,...,N-1; j = 0,1,2,...,n_{time}\}$* over $[0,T] = [0, t_{N-1,n_{time}}]$, the objective function may be taken as

$$F(\mathbf{X}) = \max_{k=1,2,3} \{\max_{i,j} |f_k(t_{i,j})| \ , \ i = 0,1,2,...,N-1; \ j = 0,1,2,...,n_{time}\} \qquad (4.4)$$

The occurrence of singularities inside the workspace of Gough-Stewart platforms is associated with dramatic increases in actuator forces [59]. Minimizing the above objective function will push the design

* note that $t_{i,0} = t_{i-1,n_{time}}$

towards an optimum platform geometry which avoids close proximity to singularities as a specific prescribed path is traced.

Apart from the fact that the objective function is dependent on the prescribed path, it is also shown in Section 4.3 that expression (2.124) is indeed an implicit function of the vector of design variables $\mathbf{X} = [X_1, X_2, X_3, X_4, X_5]^T$, and that the objective function is therefore well defined.

4.2.3 Constraints applicable on the planar machining center

With reference to Figure 4.1, the allowable relative distances between the linearly adjustable revolute joints of the fixed base (X_2 and X_5) and the moving platform (X_1) are subject to physical *lower* ($\underline{X}_i$, $i = 1,2,5$) and *upper* ($\overline{X}_i$, $i = 1,2,5$) bounds, i.e.

$$\underline{X}_i \le X_i \le \overline{X}_i,\ i = 1,2,5 \tag{4.5}$$

Similarly, the actuator leg lengths ($\ell_i, i = 1,2,3$) are bounded by *minimum* ($\underline{\ell}_i$, $i = 1,2,3$) and *maximum* ($\overline{\ell}_i, i = 1,2,3$) leg length limits:

$$\underline{\ell}_i \le \ell_i \le \overline{\ell}_i,\ i = 1,2,3 \tag{4.6}$$

These bounds are defined as the *mechanism configurational constraints*, and determine its *working capability*, since for any specific *operational geometry* $\mathbf{X} = [X_1, X_2, X_3, X_4, X_5]^T$ to be feasible, the *mechanism configurational constraints* (4.5) and (4.6) must be satisfied.

The formulation of the constrained optimization problem (expression (4.1)) allows for the easy imposition of the above configurational constraints, since they may readily be expressed as general inequality constraints of the form $C_j(\mathbf{X}) \le 0$, $(j = 1,2,3,\ldots,m)$.

In particular, expression (4.5) represents the first six inequality constraints $C_j(\mathbf{X}) \le 0$, $(j = 1,2,3,\ldots,6)$:

$$\begin{aligned} C_1(\mathbf{X}) &\equiv X_1 - \overline{X}_1 \le 0 \\ C_2(\mathbf{X}) &\equiv \underline{X}_1 - X_1 \le 0 \\ C_3(\mathbf{X}) &\equiv X_2 - \overline{X}_2 \le 0 \\ C_4(\mathbf{X}) &\equiv \underline{X}_2 - X_2 \le 0 \\ C_5(\mathbf{X}) &\equiv X_5 - \overline{X}_5 \le 0 \\ C_6(\mathbf{X}) &\equiv \underline{X}_5 - X_5 \le 0 \end{aligned} \tag{4.7}$$

The leg length limits $\underline{\ell}_i \le \ell_i \le \overline{\ell}_i$, $i = 1,2,3$ (expression (4.6)) represent an additional six inequality constraints $C_{j+6}(\mathbf{X}) \le 0$, $(j = 1,2,3,...,6)$. As with the objective function (4.4), these six inequality constraints are dependent on the prescribed path, as well as the design variables $\mathbf{X} = [X_1, X_2, X_3, X_4, X_5]^T$ (see Section 4.3). Monitoring the prescribed path and corresponding platform geometry at discrete time instants $t_{i,j}$, the overall maximum and minimum actuator leg lengths may be obtained. They are respectively given by $\ell_k^{max}(\mathbf{X}) = \max_{i,j}[\ell_k(t_{i,j}, \mathbf{X})]$ and $\ell_k^{min}(\mathbf{X}) = \min_{i,j}[\ell_k(t_{i,j}, \mathbf{X})]$ for $k = 1,2,3$ and $\{t_{i,j}, i = 0,1,2,...,N-1; j = 0,1,2,...,n_{time}\}$ suitably small *monitoring* time intervals as previously defined in Section 4.2.2. The *allowable* maximum and minimum actuator leg lengths are respectively denoted by $\overline{\ell}_k$ and $\underline{\ell}_k$, $k = 1,2,3$, resulting in the following six mathematically expressed inequality constraints:

$$
\begin{aligned}
C_{k+6}(\mathbf{X}) &\equiv \ell_k^{max}(\mathbf{X}) - \overline{\ell}_k \le 0, \quad k = 1,2,3 \\
\text{and } C_{k+9}(\mathbf{X}) &\equiv \underline{\ell}_k - \ell_k^{min}(\mathbf{X}) \le 0, \quad k = 1,2,3
\end{aligned}
\tag{4.8}
$$

4.3 Evaluation of the constrained optimization problem

The formulated constrained optimization problem (Section 4.2) is evaluated for a specific prescribed path, given any arbitrary design $\mathbf{X} = [X_1, X_2, X_3, X_4, X_5]^T$. The design vector $\mathbf{X}$ fixes the operational geometry of the platform.

4.3.1 Evaluation of the objective function

Evaluating the objective function (4.4), involves performing a kinematic and kinetic analysis of the planar Gough-Stewart platform as explained in **Chapter 2**. In particular, for any time instant along the prescribed path, the position (x_1, y_1) and orientation (ϕ_1) of the moving platform (body 1 in Figure 2.5) are known (see Section 2.4). Furthermore, with the *operational geometry* $(\mathbf{X})$ fixed, expression (4.2) yields the local ξ_1^A- and ξ_1^B-coordinates while expression (4.3) yields global coordinates (x^C, y^C), (x^D, y^D) and (x^E, y^E). Note that since the coordinates (x^A, y^A) and (x^B, y^B) follow from (x_1, y_1, ϕ_1), ξ_1^A and ξ_1^B in expression (2.57), expressions (2.58) – (2.61) may be solved for. Expressions (2.57) – (2.61) uniquely define the coordinate vector $\mathbf{q} = [x_1, y_1, \phi_1, x_2, y_2, \phi_2, ..., x_8, y_8, \phi_8]^T$, which uniquely defines the Jacobian matrix of the planar Gough-Stewart platform given by expression (2.62). The Jacobian matrix is used to find the accelerations of the individual bodies (expression (2.56)). With these accelerations known, the Jacobian matrix is again used to solve the inverse dynamic equations of motion (expression (2.124)) for the unknown LaGrange multipliers $\boldsymbol{\lambda}$ and actuator forces **ff**.

The sensitivity of the objective function (4.4) to each of the design variable X_i, $i = 1,2,...,5$ may also be graphically determined. This is done by fixing four of the five design variables, and varying the fifth while evaluating the objective function value.

As an example, the sensitivity analysis is done for a path where the center of mass of the moving platform follows a straight-line prescribed path inclined at 60° to the horizontal as shown in Figure 4.2. Five equally spaced nodal points are used to specify the path, and using the OCAS-algorithm, the trajectory-planning is done for a specified constant tangential speed of $0.01\,\mathrm{m/s}$. Furthermore, the default time discretization parameter, $n_{time} = 10$, is used resulting in a total of 41 monitoring time intervals.

The direction of travel is such that the initial configuration of the mechanism corresponds to the one shown in dashed lines in Figure 4.2 and the final configuration to the one in solid lines. Furthermore, the moving platform remains horizontal as the straight-line path is traced. The fixed values of the respective design variables are

$$X_1 = 0.4\,\mathrm{m} \qquad X_2 = 0.4\,\mathrm{m} \qquad X_3 = -0.4\,\mathrm{m} \qquad X_4 = -0.4\,\mathrm{m} \qquad X_5 = 0.2\,\mathrm{m} \qquad (4.9)$$

and the mass matrix of this example platform is given by expression (2.132).

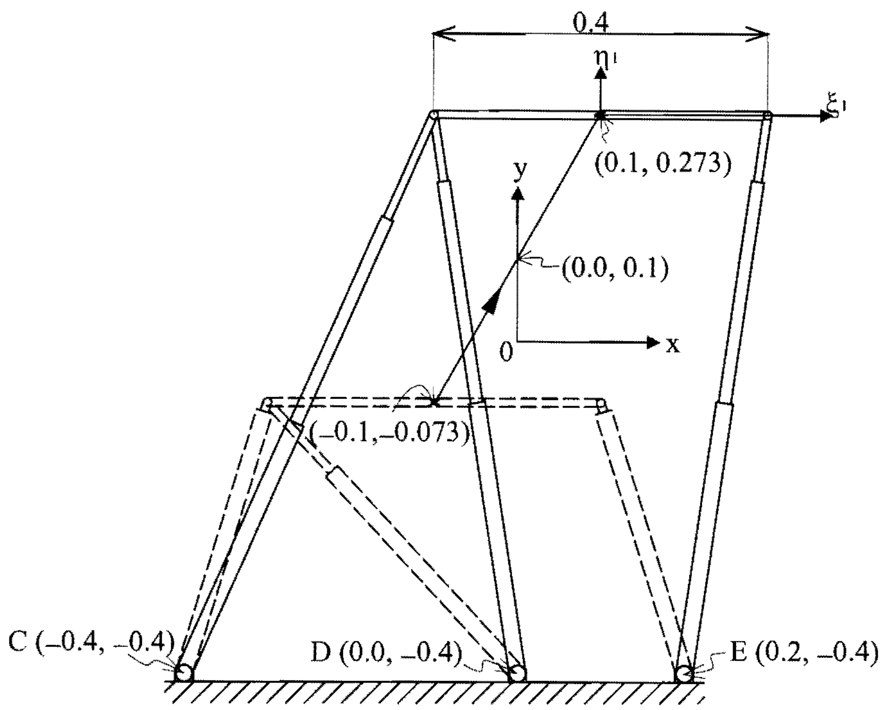

Figure 4.2: Straight-line prescribed path.

The sensitivity of the objective function to design variable X_1 is shown in Figure 4.3. Here X_1 is varied with a step size of $0.0025\,\text{m}$ between $0.1\,\text{m}$ and $1.0\,\text{m}$, while design variables X_2, X_3, X_4 and X_5 remain fixed (see expression (4.9)).

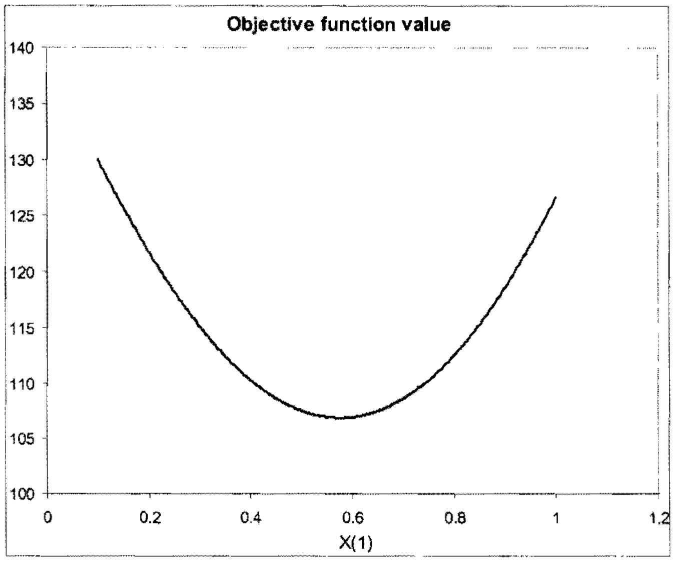

Figure 4.3: Objective function (4.4) versus design variable X_1.

Figure 4.3 consists of a *single smooth* curve, indicating that as X_1 varies, a *single* actuator is responsible for carrying the maximum magnitude actuator force. For the example prescribed path considered here (Figure 4.2), actuator leg ℓ_1 (see Figure 4.1) carries the maximum magnitude actuator force.

Evaluating the objective function while varying design variable X_1 with a step size of $0.000001\,\text{m}$ between $0.5756\,\text{m}$ and $0.576\,\text{m}$, magnifies the curve as shown in Figure 4.4. This curve demonstrates the effective absence of any numerical noise in the analysis.

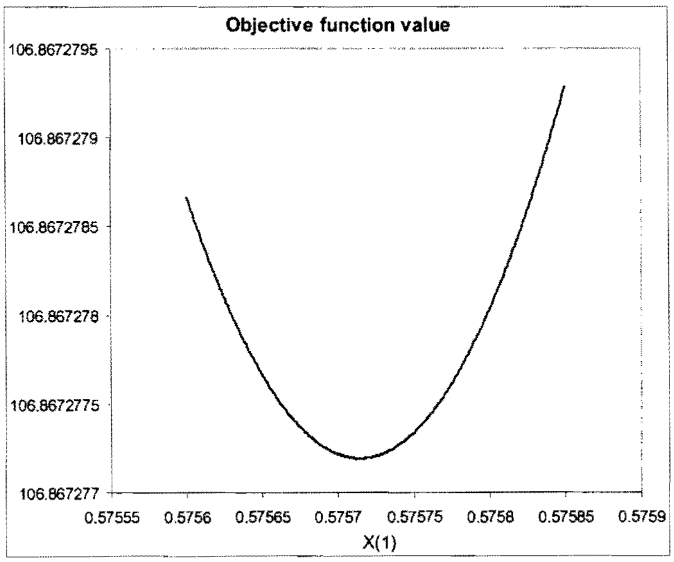

Figure 4.4: Close-up of objective function (4.4) versus design variable X_1.

This absence of noise is due to the fact that the objective function (expression (4.4)) is determined with high accuracy using the fundamentally based inverse dynamic analysis procedure explained in **Chapter 2**.

The sensitivity of the objective function to X_2 is shown in Figure 4.5. Here design variables X_1, X_3, X_4 and X_5 remain fixed (see expression (4.9)) while X_2 is varied with a step size of $0.0025\,\text{m}$ between $0.1\,\text{m}$ and $1.0\,\text{m}$.

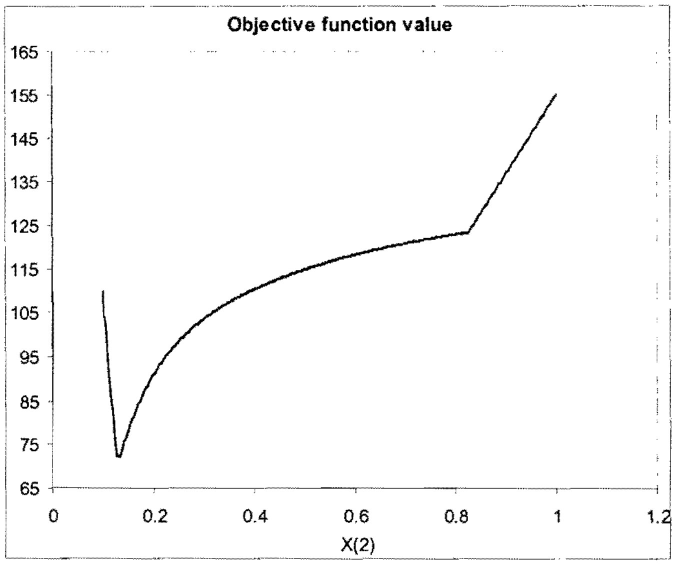

Figure 4.5: Objective function (4.4) versus design variable X_2.

In contrast to Figure 4.3 which consists of a *single* smooth curve, Figure 4.5 consists of *four* smooth curves linked to each other at three points where discontinuities in the slope (kinks) occur. Each of the three kinks in the above graph is due to a *switch* in the actuator leg responsible for the maximum magnitude actuator force.

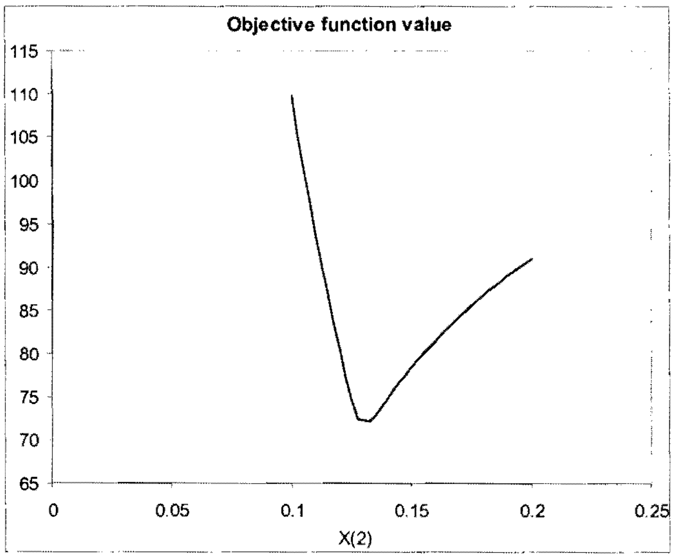

Figure 4.6: Close-up of objective function (4.4) versus design variable X_2.

Figure 4.6 shows a close-up view of the first two kinks, where the *left most* smooth curve represents actuator leg ℓ_2 (see Figure 4.1) carrying the maximum magnitude actuator force, the *middle* smooth curve represents actuator leg ℓ_3 carrying the maximum magnitude actuator force, and the *right most* smooth curve represents actuator leg ℓ_1 carrying the maximum magnitude actuator force. The isolated discontinuity in Figure 4.5 occurring near $X_2 = 0.8\,\text{m}$ is due to the switch between actuator legs ℓ_1 and ℓ_2 in carrying the maximum magnitude actuator force.

The respective sensitivities of the objective function (4.4) to design variables X_3, X_4 and X_5 are as shown in, Figures 4.7 – 4.9.

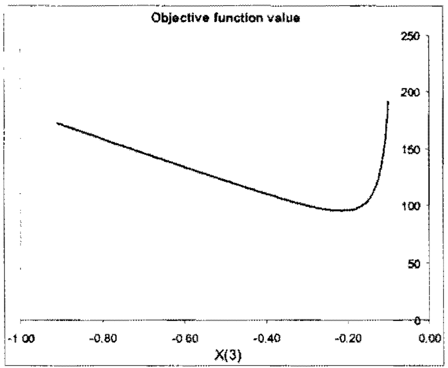

Figure 4.7: Objective function (4.4) versus design variable X_3.

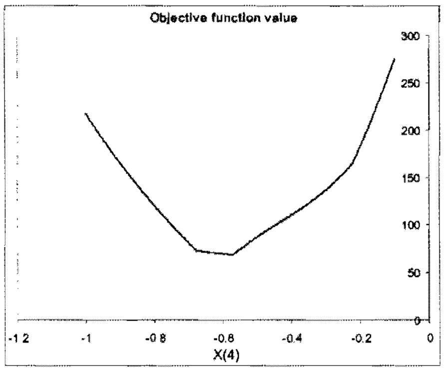

Figure 4.8: Objective function (4.4) versus design variable X_4.

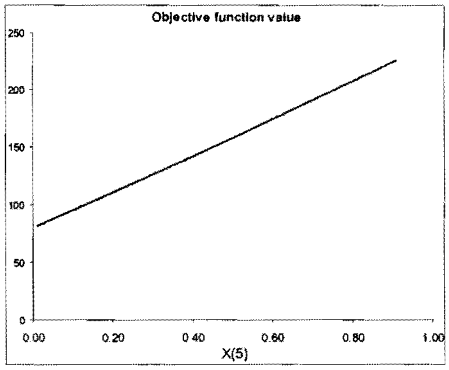

Figure 4.9: Objective function (4.4) versus design variable X_5.

4.3.2 Evaluation of the inequality constraints

Inequality constraints (4.7) may, of course, be explicitly evaluated. The evaluation of the inequality constraints (4.8) follow from the kinematic and kinetic analysis mentioned in Section 4.3.1. With the global coordinates of points A, B, C, D and E known at any time instant t, actuator leg lengths $\ell_1(\mathbf{X},t)$, $\ell_2(\mathbf{X},t)$ and $\ell_3(\mathbf{X},t)$ are the magnitudes of respective vectors $\overrightarrow{\mathbf{CA}}$, $\overrightarrow{\mathbf{DA}}$ and $\overrightarrow{\mathbf{EB}}$ (see Figure 4.1):

$$\begin{aligned}
\ell_1(\mathbf{X},t) &= \left|\overrightarrow{\mathbf{CA}}\right| = \sqrt{(x^A - x^C)^2 + (y^A - y^C)^2} \\
\ell_2(\mathbf{X},t) &= \left|\overrightarrow{\mathbf{DA}}\right| = \sqrt{(x^A - x^D)^2 + (y^A - y^D)^2} \qquad (4.10) \\
\ell_3(\mathbf{X},t) &= \left|\overrightarrow{\mathbf{EB}}\right| = \sqrt{(x^B - x^E)^2 + (y^B - y^E)^2}
\end{aligned}$$

Note that mechanism configurational constraint (4.6), not only fixes the *allowable* maximum and minimum actuator leg lengths, but also influences the kinematic and kinetic performance of the planar

Gough-Stewart platform. This follows from the relationship existing between the physical dimensions of the two bodies comprising an actuator leg, and the allowable relative actuator displacement.

Consider translational joint $2-5$, which is the left most actuator leg of the planar Gough-Stewart platform as shown in Figure 2.5 (actuator leg ℓ_1 in Figure 4.1). The physical dimensions of bodies 2 and 5 determine the allowable actuator displacement of leg 1. Furthermore, the local $0_2\xi_2\eta_2$ and $0_5\xi_5\eta_5$ coordinate systems are chosen with 0_2 and 0_5 respectively coinciding with the centers of mass of bodies 2 and 5, the positions of which are also determined by the physical dimensions of these two bodies. With the positions of the respective centers of mass of bodies 2 and 5 known, local coordinates ξ_2^A and ξ_5^C are also known. Similar arguments apply for translational joints $3-6$ and $4-7$.

With reference to Figure 2.5, local coordinates ξ_3^A and ξ_6^D of translational joint $3-6$, ξ_4^B and ξ_7^D of translational joint $4-7$, together with local coordinates ξ_2^A and ξ_5^C of translational joint $2-5$ are required to solve for expression (2.61).

4.4 Solving the constrained optimization problem

As mentioned in Section 4.1, the LFOPC-algorithm [64] is used here to optimize the adjustable geometry of the planar Gough-Stewart platform machining center for any specific prescribed path. The optimization procedure is schematically represented in Figure 4.10.

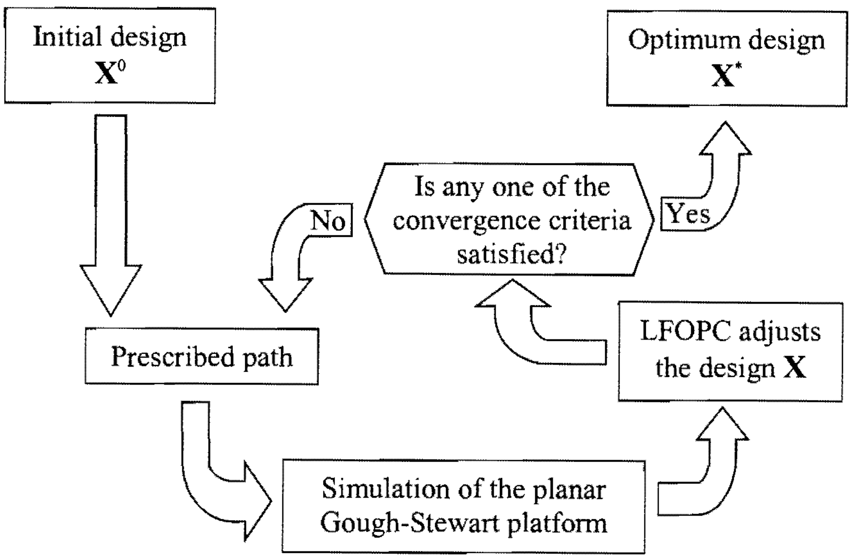

Figure 4.10: Optimization of the adjustable geometry of the planar platform machining center.

The user specifies the initial design $\mathbf{X}^0$ as well as the prescribed path. The simulation of the planar Gough-Stewart platform involves the OCAS trajectory-planning algorithm presented in **Chapter 3**, as well as the kinematic and kinetic analysis of **Chapter 2**.

The LFOPC optimization algorithm [64] used here is a *gradient-based* method for unconstrained minimization applied to a *penalty function* formulation of the constrained optimization problem. A more detailed description of the LFOPC-algorithm is given in **Appendix C**. In short, a *penalty function* is created by combining the objective function (4.4) and the inequality constraint equations (4.7) and (4.8). Furthermore, the *gradient vector* of the penalty function determines the adjustment of the design vector $\mathbf{X}$ as the LFOPC-algorithm searches iteratively for an optimum design $\mathbf{X}^*$. These optimization iterations continue until one of the following two *convergence criteria* (see Figure 4.10) is satisfied:

1. The norm of the penalty function gradient vector is below a specified value ε_g
2. The norm of the relative design vector, given by $\left\|\mathbf{X}^{\text{"Current"}} - \mathbf{X}^{\text{"Previous"}}\right\|$, is below a specified tolerance ε_x.

In determining the gradient vector of the penalty function, LFOPC requires the gradient vector of the objective function with respect to the design variables, as well as the gradient vectors of each inequality constraint with respect to the design variables.

The gradient vector of the objective function (4.1) with respect to the design variables is obtained by differentiating numerically using forward finite differences [55]. The components of the objective function gradient vector at any specific design $\mathbf{X} = [X_1, X_2, X_3, X_4, X_5]^T$ is approximated by

$$\frac{\partial F(\mathbf{X})}{\partial X_i} \approx F\left[\mathbf{X} + \Delta\mathbf{X}_i, \mathbf{X}\right] = \frac{F(\mathbf{X} + \Delta\mathbf{X}_i) - F(\mathbf{X})}{\varepsilon_i} \tag{4.11}$$

where $\Delta\mathbf{X}_i = [0,0,\ldots,\varepsilon_i,\ldots,0]^T$ with $\varepsilon_i > 0$ in the i^{th} position, and $i = 1,2,\ldots,5$.

With reference to the optimization flowchart given in Figure 4.10, six simulation runs of the planar Gough-Stewart platform are required per iteration. This is because at each design point forward finite differences are used in computing the gradient components of the objective function, requiring five *perturbed* objective function values, and one *unperturbed* objective function value as is apparent from expression (4.11).

The appropriate values of ε_i to be used may be determined from an experimental sensitivity study of the approximate gradients with respect to different step sizes ε_i of the five design variables. For any chosen design **X**, the objective function may be determined as the platform traces the prescribed path. The sensitivity of, for example the variation of the approximation $F[\mathbf{X}+\Delta\mathbf{X}_i,\mathbf{X}]$ to $\dfrac{\partial F(\mathbf{X})}{\partial X_i}$ with respect to different orders of magnitude of ε_i, may be represented by an exponential graph. The graph of $F[\mathbf{X}+\Delta\mathbf{X}_i,\mathbf{X}]$ versus ε_i is expected to show a stable plateau, the mid ε-value of which is the most suitable value to be used in expression (4.11).

A sensitivity analysis of $F[\mathbf{X}+\Delta\mathbf{X}_i,\mathbf{X}]$ versus ε_i is performed here for the example straight-line prescribed path shown in Figure 4.2. For this sensitivity analysis, a constant tangential speed of 0.1 m/s is specified, and the moving platform remains horizontal as the prescribed path is traced. The fixed design of the adjustable geometry planar Gough-Stewart platform at which the sensitivity analysis is performed is $\mathbf{X}=[0.4,0.4,-0.4,-0.4,0.2]^T$ (see Figure 4.2) and the mass matrix of this example platform is given by expression (2.132).

The computed approximations $F[\mathbf{X}+\Delta\mathbf{X}_i,\mathbf{X}]$ (denoted by $F[\mathbf{X}+\Delta\mathbf{X}\_i,\mathbf{X}]$) to the gradients $\dfrac{\partial F(\mathbf{X})}{\partial X_i}$, $i=1,2,\ldots,5$ are plotted versus ε in Figure 4.11.

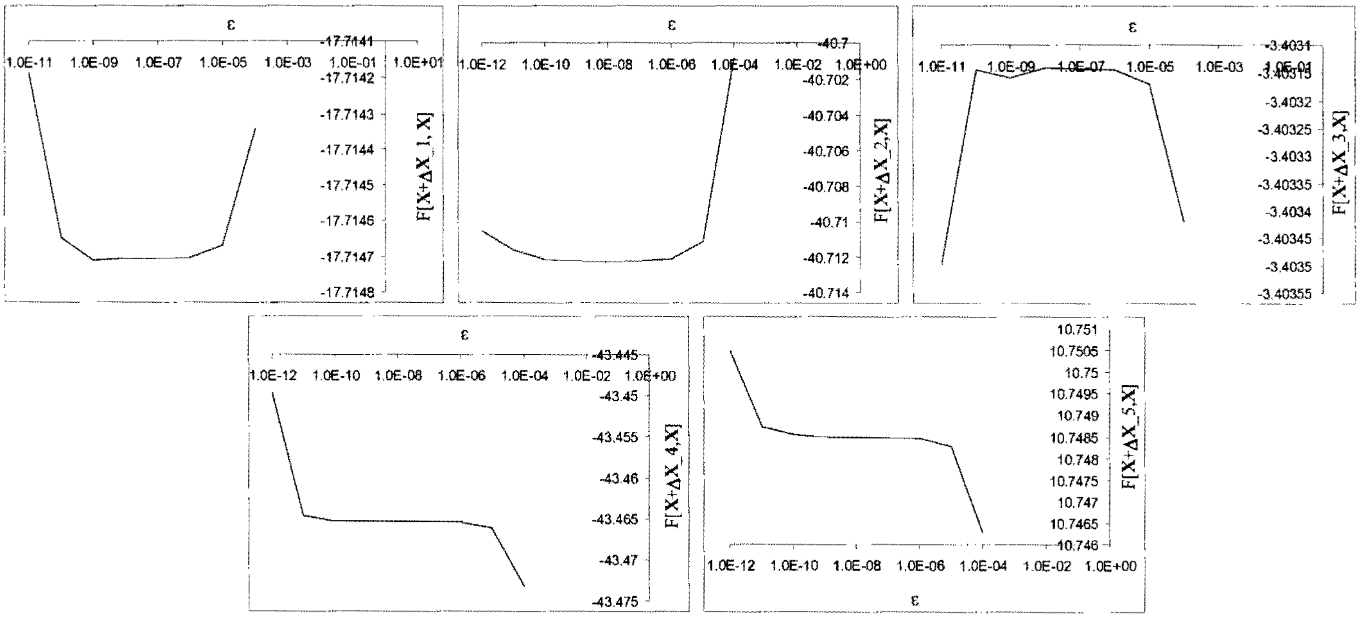

Figure 4.11: Sensitivity of $F[\mathbf{X}+\Delta\mathbf{X}_i,\mathbf{X}]$ to step size ε, for $i=1,2,\ldots,5$.

The above sensitivity analyses show that the choice $\varepsilon_i \equiv \varepsilon = 10^{-8}$, $i=1,2,\ldots,5$ will result in reliable computed gradients.

The components of the gradient vectors of each inequality constraint function in (4.7) are, of course, analytically known and given by:

$$\begin{array}{lllll}
\frac{\partial C_1(\mathbf{X})}{\partial X_1}=1 & \frac{\partial C_1(\mathbf{X})}{\partial X_2}=0 & \frac{\partial C_1(\mathbf{X})}{\partial X_3}=0 & \frac{\partial C_1(\mathbf{X})}{\partial X_4}=0 & \frac{\partial C_1(\mathbf{X})}{\partial X_5}=0 \\
\frac{\partial C_2(\mathbf{X})}{\partial X_1}=-1 & \frac{\partial C_2(\mathbf{X})}{\partial X_2}=0 & \frac{\partial C_2(\mathbf{X})}{\partial X_3}=0 & \frac{\partial C_2(\mathbf{X})}{\partial X_4}=0 & \frac{\partial C_2(\mathbf{X})}{\partial X_5}=0 \\
\frac{\partial C_3(\mathbf{X})}{\partial X_1}=0 & \frac{\partial C_3(\mathbf{X})}{\partial X_2}=1 & \frac{\partial C_3(\mathbf{X})}{\partial X_3}=0 & \frac{\partial C_3(\mathbf{X})}{\partial X_4}=0 & \frac{\partial C_3(\mathbf{X})}{\partial X_5}=0 \\
\frac{\partial C_4(\mathbf{X})}{\partial X_1}=0 & \frac{\partial C_4(\mathbf{X})}{\partial X_2}=-1 & \frac{\partial C_4(\mathbf{X})}{\partial X_3}=0 & \frac{\partial C_4(\mathbf{X})}{\partial X_4}=0 & \frac{\partial C_4(\mathbf{X})}{\partial X_5}=0 \\
\frac{\partial C_5(\mathbf{X})}{\partial X_1}=0 & \frac{\partial C_5(\mathbf{X})}{\partial X_2}=0 & \frac{\partial C_5(\mathbf{X})}{\partial X_3}=0 & \frac{\partial C_5(\mathbf{X})}{\partial X_4}=0 & \frac{\partial C_5(\mathbf{X})}{\partial X_5}=1 \\
\frac{\partial C_6(\mathbf{X})}{\partial X_1}=0 & \frac{\partial C_6(\mathbf{X})}{\partial X_2}=0 & \frac{\partial C_6(\mathbf{X})}{\partial X_3}=0 & \frac{\partial C_6(\mathbf{X})}{\partial X_4}=0 & \frac{\partial C_6(\mathbf{X})}{\partial X_5}=-1
\end{array} \qquad (4.12)$$

On the other hand, the forward finite difference formula is again used to numerically approximate the derivatives of the inequality constraint functions in (4.8) at any given design $\mathbf{X}=[X_1,X_2,X_3,X_4,X_5]^T$:

$$\frac{\partial C_{j+6}(\mathbf{X})}{\partial X_i} \approx C_{j+6}[\mathbf{X}+\Delta\mathbf{X}_i,\mathbf{X}] = \frac{C_{j+6}(\mathbf{X}+\Delta\mathbf{X}_i)-C_{j+6}(\mathbf{X})}{\varepsilon_i} \qquad (4.13)$$

where $\Delta\mathbf{X}_i=[0,0,...,\varepsilon_i,...,0]^T$ with $\varepsilon_i>0$ in the i^{th} position, and $j=1,2,...,6$.

The same six simulation runs of the planar Gough-Stewart platform required to determine the objective function gradient vector, are utilized to evaluate expression (4.13).

The gradients of the inequality constraint functions are expected to have similar sensitivities with respect to the order of magnitude of ε_i as the objective function gradients (see Figure 4.11), hence $\varepsilon_i \equiv \varepsilon = 10^{-8}$ is used in expression (4.13), for all j.

4.5 Discussion of optimization results

The prescribed straight-line path of Figure 4.2 is used here to *illustrate* the determination of the optimum geometry of the planar Gough-Stewart platform machining center for a given task path. Using the *general* OCAS trajectory-planning methodology (see **Chapter 3**), the straight-line path is prescribed by specifying 5 nodal points as shown in Figure 4.12. Again the default value of $n_{time}=10$ is used for the discretization parameter in the analysis of the straight-line path.

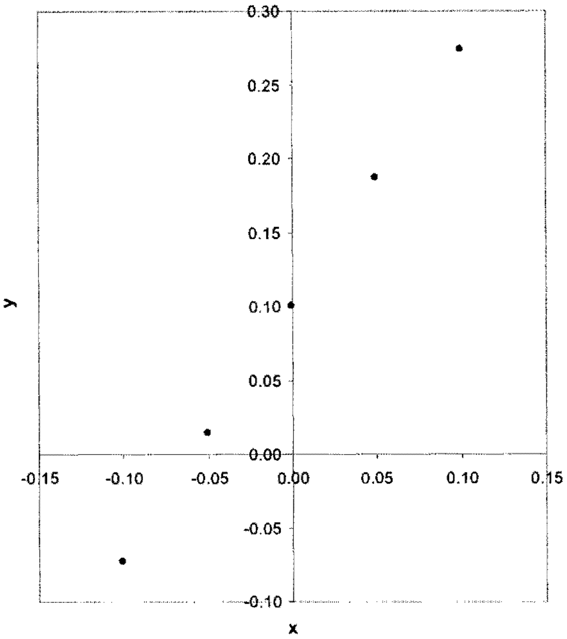

Figure 4.12: Nodal points specified for the straight-line prescribed path.

For this illustrative example, the "fixed workpiece" mode of operation of the machining center, as explained in Sections 2.4.1 and 2.6.4.2.1, is used with a zero tool length $\eta_1^P = 0.0$. Specifying a zero tool length enforces the center of mass of the moving platform to trace the prescribed straight-line path, as was done for the sensitivity analysis explained in Section 4.3.1. Furthermore, a fixed moving platform orientation $\phi_1 \equiv 0$ (see Figure 4.2) is maintained with a *constant* tangential cutting speed of $0.01\,\text{m/s}$ and a "cutting force constant" $C_{cut} = 10000\,\text{Ns/m}$ (see expression (2.107)). Since the length of the prescribed straight-line path is $0.4\,\text{m}$, the motion takes $40\,\text{s}$ to complete.

With reference to Figure 4.1 the initial configuration of the planar machining center is $\mathbf{X}^0 = [0.4,\ 0.4,\ -0.4,\ -0.4,\ 0.2]^T$, where the design variables X_1^0, X_2^0 and X_5^0 (given in m) are in scaled agreement with the geometry of Haug et al.'s [73] planar Gough-Stewart platform. The initial coordinates $(X_4^0;\ X_3^0)$ of the left- most revolute joint on the horizontal base are arbitrarily chosen as $(-0.4;\ -0.4)$. Figure 4.2 is a *scaled* schematic representation of the machining center fixed to these initial geometry settings $\mathbf{X}^0 = [0.4,\ 0.4,\ -0.4,\ -0.4,\ 0.2]^T$ at the start and end points of the prescribed straight-line path. The mass matrix of this platform is again given by expression (2.132).

Figure 4.14 shows the variation in the respective actuator lengths (designated by L1, L2 and L3) as the prescribed path is followed using the initial design, while Figure 4.16 shows the variation of corresponding actuator forces f_k, $k = 1,2,3$ (designated by f1, f2 and f3) for the prescribed path.

It is important to note that the allowable maximum actuator lengths $\bar{\ell}_k = 0.525$ m, $k = 1,2,3$ designated by Lmax in Figure 4.14 are violated if the initial design is used to trace the prescribed path. These violations imply that the specified tool path lies outside the workspace of the platform and that the initial geometry settings are therefore *infeasible* for carrying out the prescribed task. The specific bounds of the *mechanism configurational constraints*, given in meters, (see Section 4.2.3, expressions (4.5) and (4.6)), are

$$\begin{gathered} 0.1 \le X_1 \le 0.45 \\ 0.113 \le X_2 \le 0.465 \\ 0.113 \le X_5 \le 0.27 \end{gathered} \tag{4.14}$$

and

$$0.075 \le \ell_i \le 0.525,\ i = 1,2,3 \tag{4.15}$$

In particular, the inequality constraint function values for tracing the straight-line prescribed tool path using the initial design $\mathbf{X}^0$, are

$$\begin{array}{lll} C_1(\mathbf{X}^0) = -0.05 & C_2(\mathbf{X}^0) = -0.3 & C_3(\mathbf{X}^0) = -0.065 \\ C_4(\mathbf{X}^0) = -0.287 & C_5(\mathbf{X}^0) = -0.07 & C_6(\mathbf{X}^0) = -0.087 \\ \to C_7(\mathbf{X}^0) = 0.21202 & \to C_8(\mathbf{X}^0) = 0.15559 & \to C_9(\mathbf{X}^0) = 0.15559 \\ C_{10}(\mathbf{X}^0) = -0.26675 & C_{11}(\mathbf{X}^0) = -0.36862 & C_{12}(\mathbf{X}^0) = -0.26675 \end{array}$$

where the violated inequality constraints associated with the initial design $\mathbf{X}^0$ have function values greater than zero, and are indicated by a *single* arrow $\to$.

The optimized geometry settings for the straight-line prescribed path are: $\mathbf{X}^* = [0.44978,\ 0.34151,\ -0.14924,\ -0.38010,\ 0.13973]^T$. Figure 4.13 shows a scaled schematic representation of the machining center fixed to these optimal geometry settings at the start and end points of the prescribed straight-line path. Figure 4.15 shows the variation in the actuator lengths for the optimum platform design. The varying actuator lengths lie well within the minimum and maximum bounds specified, demonstrating the feasibility of the optimum design $\mathbf{X}^*$. The particular inequality constraint function values for tracing the straight-line prescribed tool path using the optimum design $\mathbf{X}^*$, are

$$\begin{array}{lll} C_1(\mathbf{X}^*) = -0.223\times 10^{-3} & C_2(\mathbf{X}^*) = -0.34978 & C_3(\mathbf{X}^*) = -0.12349 \\ C_4(\mathbf{X}^*) = -0.22851 & C_5(\mathbf{X}^*) = -0.13027 & C_6(\mathbf{X}^*) = -0.02673 \\ C_7(\mathbf{X}^*) = -0.03145 & C_8(\mathbf{X}^*) = -0.09383 & C_9(\mathbf{X}^*) = -0.04696 \\ C_{10}(\mathbf{X}^*) = -0.01897 & C_{11}(\mathbf{X}^*) = -0.21098 & C_{12}(\mathbf{X}^*) = -0.00466 \end{array}$$

Note that since all the above inequality constraint function values are less than zero, the optimum design found by the LFOPC-algorithm is referred to as an *unconstrained optimum*. In the event that the optimum solution corresponds to a design where one or more inequality constraint function values are equal to zero, the associated constraints are considered *active*, and the design $\mathbf{X}^*$ is known as a *constrained optimum*. In the actual practical numerical identification of active constraints, the condition *equal to zero* is relaxed to *approximately equal to zero*.

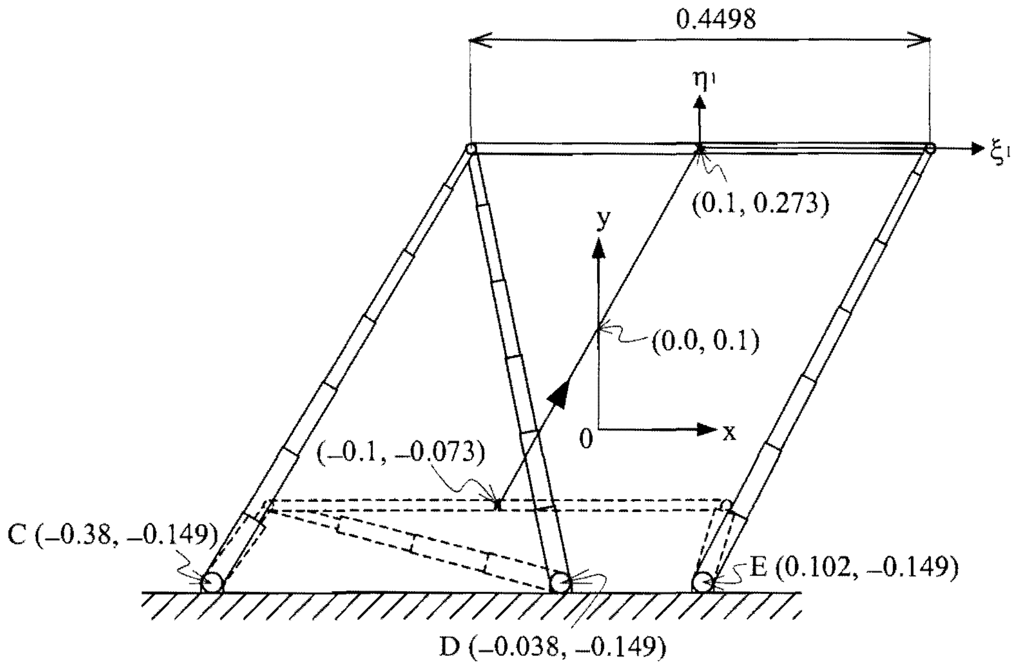

Figure 4.13: Scaled schematic representation of optimum machining center geometry settings.

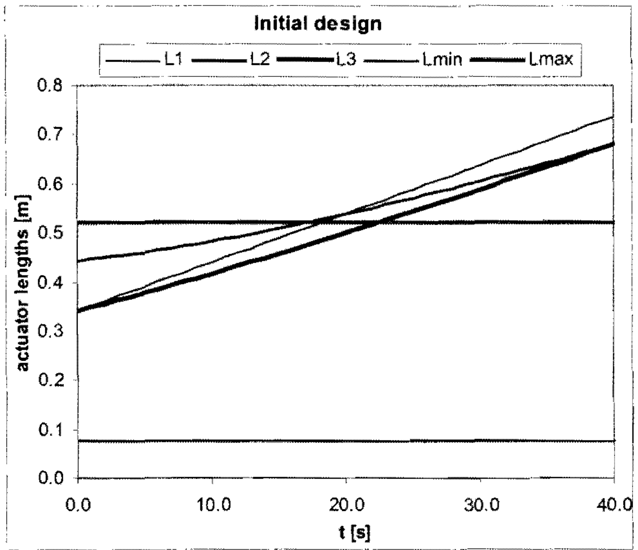

Figure 4.14: Initial design: variation of actuator lengths along tool path.

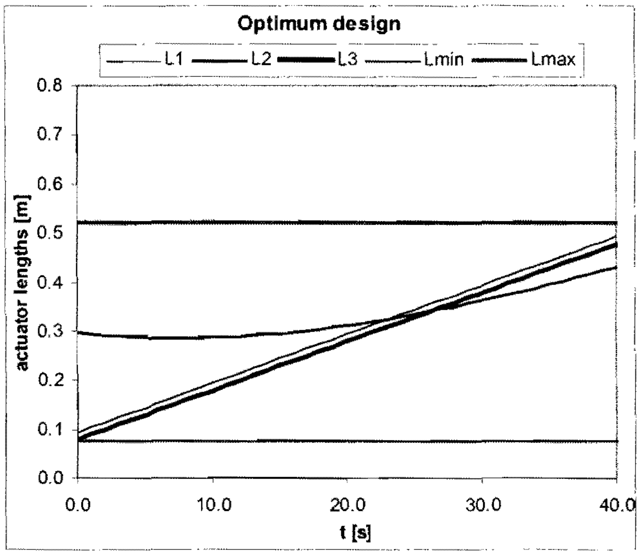

Figure 4.15: Optimum design: variation of actuator lengths along tool path.

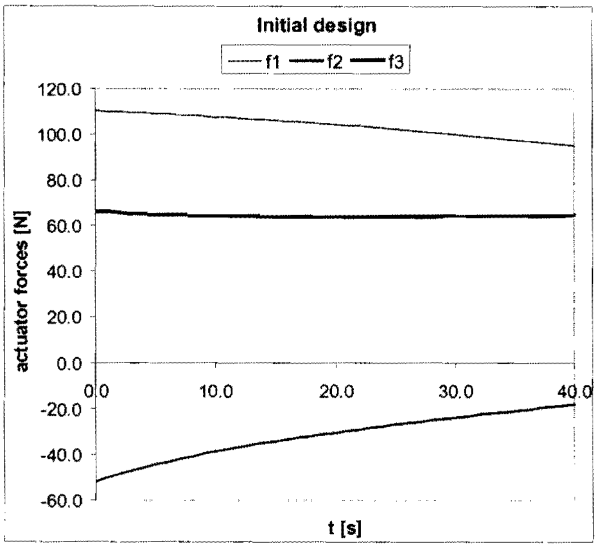

Figure 4.16: Initial design: variation of actuator forces along tool path.

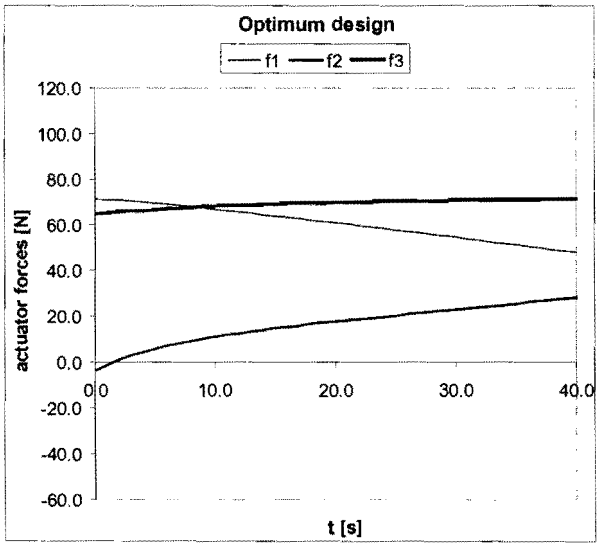

Figure 4.17: Optimum design: variation of actuator forces along tool path.

The effectiveness of the optimization procedure is further borne out by comparing Figure 4.16, with Figure 4.17, showing the variations in actuator forces for the optimum and initial designs respectively. For this simple illustrative example, the objective function value (expression (4.4)) is reduced by approximately 35% by optimizing the geometry of the platform. The initial objective function value is $F(\mathbf{X}^0) = 110.28$ N in actuator leg 1, compared to the optimum objective function value of $F(\mathbf{X}^*) = 71.32$ N, also in actuator leg 1.

The objective function convergence history is depicted in Figure 4.18.

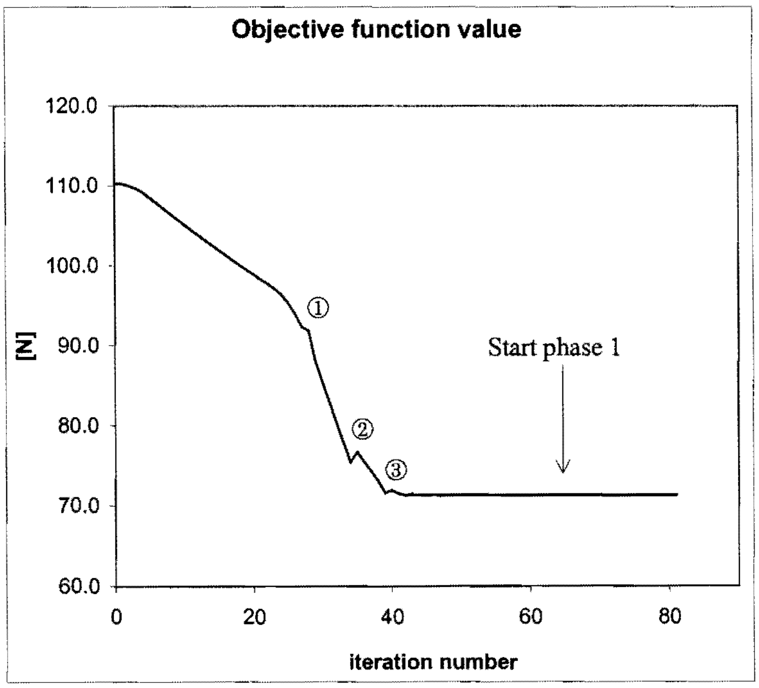

Figure 4.18: Objective function convergence history.

The labels ① – ③ in Figure 4.18 are used in Table 4.1 to relate the *iteration number* and *phase* of the LFOPC-algorithm (see **Appendix C**) to the actuator leg responsible for the *maximum magnitude actuator force* (see Section 4.2.2) and the violated inequality constraints at the indicated regions of the convergence curve.

Labels	Iter. No.	LFOPC-Phase	Act. Leg	Violated Inequality Constraints
$\mathbf{X}^0$	0	0	ℓ_1	C_7 C_8 C_9
①	25-26	0	ℓ_1	None
	27	0	ℓ_1	None
	28	0	ℓ_3	None
	29	0	ℓ_1	None
	30-32	0	ℓ_1	None
②	33	0	ℓ_1	C_1 C_{12}
	34	0	ℓ_1	C_1 C_{12}
	35	0	ℓ_1	C_1 C_{12}
	36	0	ℓ_1	C_1 C_{12}
③	39	0	ℓ_1	C_1
	40-42	0	ℓ_3	C_1
	43	0	ℓ_1	C_1
	44	0	ℓ_3	C_1
	45	0	ℓ_3	C_1
	46	0	ℓ_1	C_1
LFOPC-phase change	64	0	ℓ_3	C_1
	65	0	ℓ_1	C_1 violated constraint value $C_1(\mathbf{X}^{65}) = 0.570 \times 10^{-3}$
	65	1	ℓ_1	C_1
	66	1	ℓ_1	C_1
	80	1	ℓ_3	None
$\mathbf{X}^*$	81	1	ℓ_1	None

Table 4.1: Comparative table for the parabolic tool path objective function vs. iteration number curve (see Figure 4.18).

Note that there are switches between actuator legs ℓ_1 and ℓ_3 in being responsible for the maximum magnitude actuator force at labels ① and ③. The discontinuities in the objective function gradient vector (4.11) associated with these switches (see Section 4.3.1) are responsible for the unsmooth behavior of objective function convergence graph in these regions. The slight spiked behavior occurring at label ② can be attributed to inequality constraints C_1 and C_{12} being violated during iterations $\mathbf{X}^{33} - \mathbf{X}^{38}$.

Figure 4.19 shows the corresponding convergence histories for the design variables X_i, $i = 1,2,...,5$.

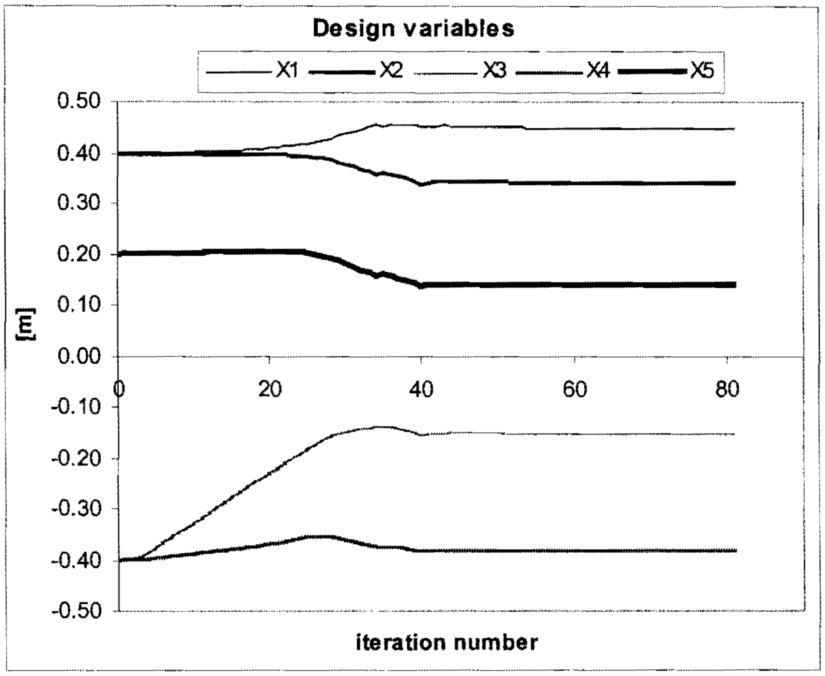

Figure 4.19: Convergence histories of design variables X_i, $i = 1,2,...,5$.

When comparing Figure 4.18 with Figure 4.19, it is evident that the LFOPC optimization algorithm [64] used here effectively converges to the optimum solution after only 50 optimization iterations. In particular, Table 4.1 shows that the end of phase 0 of the LFOPC-algorithm, the only violated constraint is C_1 with an associated constraint function value of $C_1(\mathbf{X}^{65}) = 0.570 \times 10^{-3}$ m (0.570 mm). This violation is of such small magnitude that it is negligible.

The optimum solution, corresponding to the specification of extremely accurate convergence tolerances ($\varepsilon_g = 10^{-5}$ for criterion 1; and $\varepsilon_x = 10^{-5}$ for criterion 2 in Section 4.4), is found after 81 optimization iterations and utilizing 53 seconds computational time on a Pentium IV 1.5 GHz computer with 640 MB DDRAM. The specific criterion that the LFOPC-algorithm terminated on is criterion 2, $\varepsilon_x \leq 10^{-5}$ (see Section 4.4). Throughout the choice DELT = 0.01 was used for the LFOPC maximum stepsize parameter (see **Appendix C**).